Rapid MR-ARFI Method for Focal Spot Localization During Focused Ultrasound Therapy

Elena A. Kaye,[1,2]* Jing Chen,[3] and Kim Butts Pauly[2]

MR-guided focused ultrasound (FUS) is a noninvasive therapy for treating various pathologies. MR-based acoustic radiation force imaging (MR-ARFI) measures tissue displacement in the focal spot due to acoustic radiation force. MR-ARFI also provides feedback for adaptive focusing algorithms that could correct for phase aberrations caused by the skull during brain treatments. This work developed a single-shot echo-planar imaging–based MR-ARFI method that reduces scan time and ultrasound energy deposition. The new method was implemented and tested in a phantom and ex vivo brain tissue. The effect of the phase aberrations on the ultrasound focusing was studied using displacement maps obtained with echo-planar imaging and two-dimensional spin-warp MR-ARFI. The results show that displacement in the focal spot can be rapidly imaged using echo-planar imaging–based MR-ARFI with high signal-to-noise ratio efficiency and without any measurable tissue heating. Echo-planar imaging–based displacement images also demonstrate sufficient sensitivity to phase aberrations and can serve as rapid feedback for adaptive focusing in brain treatments and other applications. Magn Reson Med 65:738–743, 2011. © 2010 Wiley-Liss, Inc.

Key words: MR-ARFI; displacement map; single-shot EPI

MR-guided focused ultrasound (FUS) is a promising noninvasive therapy in applications such as the treatments of uterine fibroids (1), breast tumors (2–4), liver tumors (5), and a range of brain pathologies (6–8). In these treatments, the therapeutic effect is achieved by delivery of high-intensity ultrasound to a target inside the body. On its way to the target, ultrasound propagates through layers of acoustically inhomogeneous tissue, which can produce phase aberrations (9) and affect the position and the quality of the focal spot. In particular, propagation through bone, such as skull and ribs, where the speed of sound is greater than in tissue, can result in such significant aberrations that the ultrasound becomes completely unfocused in the targeted area (10–12). Therefore, prior to focused ultrasound treatments, it is important to verify if the ultrasound beam is focused in the prescribed position and if not, to apply the necessary phase corrections.

[1]Department of Electrical Engineering, Stanford University, Stanford, California, USA.
[2]Department of Radiology, Stanford University, Stanford, California, USA.
[3]Institute of Biophysics, Chinese Academy of Sciences, Beijing, China.
Grant sponsor: NIH; Grant numbers: RO1 CA121163, P41 RR009784.
*Correspondence to: Elena A. Kaye, M.S., Lucas MRI Center, MC 5488, 1201 Welch Rd., Stanford, CA 94305. E-mail: klena@stanford.edu
Received 17 March 2010; revised 9 August 2010; accepted 1 September 2010.
DOI 10.1002/mrm.22662
Published online 16 November 2010 in Wiley Online Library (wileyonlinelibrary.com).

Currently during the planning stage of an MR-guided focused ultrasound procedure, a low-temperature test spot is created. The focal spot is typically visualized during a small temperature rise either with proton resonance frequency thermometry (13) or with T_1-weighted imaging (4). The transducer is next calibrated to accurately target the desired location. In the case of transcranial brain treatments, there is an additional planning step that corrects phase aberrations prior to the calibration step. This relies on a presurgical computed tomography (CT) scan of the head (6,7,10,11), which is used to measure skull bone properties and to calculate phase correction values.

An alternative method for focal spot localization that avoids heat deposition in the target would be to use tissue displacement maps obtained with MR acoustic radiation force imaging (MR-ARFI) using quasi-static approach (14–18). MR-ARFI has been described within the context of several MRI pulse sequences: line scan and two–dimensional (2D) gradient-echo and spin-warp imaging. Large unipolar gradients (14) and improved smaller bipolar gradients (17) were used in the line scan method. Smaller bipolar gradient and sinusoidal gradients were used in 2D gradient-echo and spin-warp methods (15,16). The latter two were tested in vivo in a thigh muscle of a rabbit and in a rat brain.

The ability to visualize the focal spot with MR-ARFI has also been recently explored as a feedback source in an adaptive focusing algorithm for transcranial brain treatments (19,20) designed to replace the presurgical CT scan. In this approach, the phase correction values that maximize the intensity in the focal spot are assigned to the transducer elements. The variations of intensity in the focal spot are estimated from the MR-ARFI displacement maps. To calculate the phase corrections for each of the N elements of the transducer, at least $3N$ ultrasound emissions are necessary, where $N/2$ Hadamard encoded elements are on per each emission (18). Therefore, to complete the full set of measurements $3 \times N \times 2$ MR-ARFI acquisitions are required, where a factor of 2 signifies two equivalent acquisitions with the opposite gradient polarity. Thus, the total scan time for such an algorithm quickly becomes unwieldy. Furthermore, the potential for unwanted heat deposition increases with the number of acquisitions.

To address the need for a faster MR-ARFI method as a planning tool for MR-guided focused ultrasound procedures, especially for adaptive focusing in the brain, and to reduce heat deposition, we developed a rapid MR-ARFI technique based on single-shot echo-planar imaging (EPI). Repeated bipolar displacement-encoding gradients, selected as the optimal gradients for MR-ARFI (17), were combined with a limited field of view (FOV) to accelerate focal spot displacement imaging.

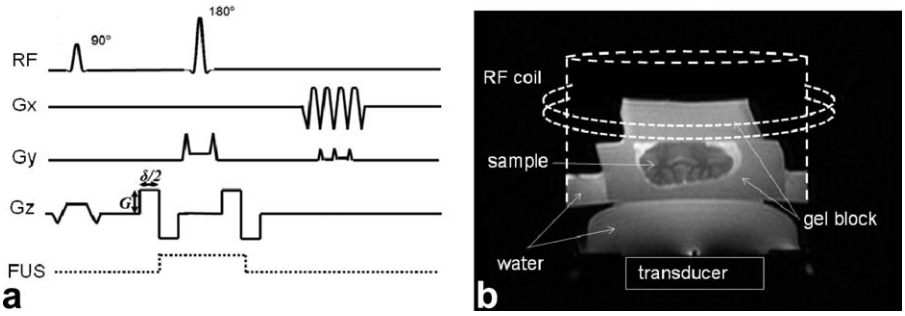

FIG. 1. **a**: Simplified pulse sequence diagram for a limited FOV single-shot flyback EPI MR-ARFI. The timing of the ultrasound pulse (FUS) is shown with the dotted line. **b**: The experimental setup showing the transducer location, tissue sample, and coil positions. The transducer is covered with a plastic membrane filled with degassed water for acoustic coupling. A plastic cylinder (dashed line), containing the sample in a coupling gel block, is placed on top of the membrane. A Mylar® membrane on the lower side of the cylinder provides coupling with the transducer while containing these materials. A second piece of gel block is located on top of the tissue.

Displacement maps were compared with those obtained using 2D spin-warp MR-ARFI. Temperature measuring capability was introduced to monitor any heating at the focal spot that could occur during MR-ARFI acquisition. To evaluate the benefits and limitations of an EPI-based MR-ARFI sequence, tests were performed in a phantom and in ex vivo porcine brain tissue.

MATERIALS AND METHODS

MR-ARFI

A single-shot flyback EPI pulse sequence was developed with a limited FOV in the phase-encode direction (18). A rectangular slab was excited by applying orthogonal slice select gradients for the 90° and 180° radio frequency (RF) pulses, as shown in Fig. 1a. Repeated bipolar displacement-encoding gradients were placed around 180° RF pulse. The amplitude of the gradients was set to 4 G cm^{-1}, and the duration of each lobe was 6.1 msec, which corresponds to the b value of 42 sec mm^{-2}. In addition, a 2D spin-warp pulse sequence was modified for MR-ARFI by including displacement-encoding gradients identical to the ones used in the EPI sequence. Imaging was performed on a 3-T MRI scanner (Signa, GE Medical Systems, Waukesha, WI). Images were acquired in coronal plane with imaging parameters listed in Table 1.

Ultrasound Transducer

MRI scanner was equipped with an MR-compatible 2D flat phased array ultrasound transducer (ExAblate® 2000, InSightec Inc, Haifa, Israel). The array had 1024 rectangular elements and a total area of 80 × 80 mm^2. It was operated at the central frequency of 550 kHz in continuous wave mode. The transducer was driven by a proprietary phased array acoustic front end, controlling the phasing of each element. MRI pulse sequences triggered the FUS system to emit ultrasound for 20.6 msec synchronously with the encoding gradients (Fig. 1a), so that for the repetition time (TR) of 1 sec, the duty cycle was 2%. The ultrasound beam was focused at a depth of 76 mm from the center of the transducer. The focal spot size at full width at half-maximum intensity at the focus was 2.8 mm in diameter and 18 mm in the beam direction based on a beam field simulation [Field II (21,22)].

Ex Vivo Experiments

The measurements were performed in either a tissue-mimicking phantom designed to match the US attenuation and speed of sound in tissue or in ex vivo porcine brain. A custom made phantom (ATS Laboratories, Bridgeport, CT) had the following properties: density = 1040 kg m^{-3}, speed of sound = 1455 m sec^{-1}, absorption coefficient = 95 dB m^{-1} MHz^{-1}, acoustic impedance = 1.54 × 10^6 kg m^{-2} sec^{-1}, amplitude reflection coefficient = 1.7 × 10^{-2}, heat capacity = 3765 J kg^{-1} K^{-1}, thermal conductivity = 0.33 W m^{-1} K^{-1} (courtesy of InSightec Inc.). The whole brain was obtained from a pig ~24 h before the experiment and was kept refrigerated. During the experiment, the degassed tissue was kept at room temperature of ~20°C.

The experimental setup is shown in Fig. 1b. The phantom or the brain in a gel block, which was made of the gelatin-based pelvic pad (InSightec Inc.), were placed into a plastic holder with a Mylar® membrane on the bottom. This cylinder was then positioned on top of the water-filled membrane over the FUS transducer. A solenoid RF coil was placed around the plastic holder.

To map the displacement, a pair of images were obtained with identical imaging and sonication parameters but with opposite polarity of the encoding gradients (14). Both phase images were unwrapped and corrected for bulk motion phase by subtracting constant and linear background phase corrections. From these images, a phase difference image was calculated and converted to displacement according to Eq. 1

$$\Delta d = \Delta\varphi/(4\pi\gamma G\delta), \quad [1]$$

where Δd is the displacement, $\Delta\varphi$ is the phase difference, γ is the proton gyromagnetic ratio, G is the

Table 1
Imaging Parameters Used in MR-ARFI Acquisitions

	EPI	2D spin warp
Bandwidth, kHz	62.5	15.6
Slice thickness, mm	3	3
FOV, mm^2	160 × 50	160 × 160
Matrix size	128 × 30	256 × 128
Echo time, msec	108	41

amplitude of the encoding gradients, and δ is the duration of two gradient lobes.

In the first demonstration of EPI-based MR-ARFI, displacement maps were obtained with the rapid EPI-based sequence in a phantom. The duty cycle was calculated as the fraction of sonication time to imaging TR in percent. Displacement images were obtained with applied acoustic power of 93, 117, and 156 W using a duty cycle of 2%. Taking into account the energy loss due to attenuation in the phantom and in the brain tissue (23), corresponding acoustic intensities (spatial peak) at the focus were estimated to be 370, 465, and 620 W cm^{-2}.

The goal of the second experiment was to measure the temperature rise in a phantom and in brain tissue after one single-shot EPI MR-ARFI acquisition and also after a set of continuously repeated 3000 MR-ARFI acquisitions. The latter was only performed in a phantom. For this experiment, the readout of the single-shot EPI was shifted from the spin echo by 8 msec to introduce temperature sensitivity and the displacement-encoding gradients were set to zero to disable displacement sensitivity. The temperature maps were calculated by subtracting a reference phase obtained from the acquisitions with the US switched off, from the phase obtained with the US switched on. The temperature rise was found from the following proton resonance frequency relationship:

$$\Delta T = \frac{\varphi(T) - \varphi(T_0)}{\gamma \alpha B_0 \Delta TE}, \qquad [2]$$

where $\varphi(T)$ is the phase of an image with US switched on and $\varphi(T_0)$ is the phase with US switched off, α is proton resonance frequency change coefficient, and B_0 is the magnetic field strength. The acoustic power levels used for the brain tissue were 31 and 62 W, and 156 W for the phantom, corresponding to estimated focal intensities of 123 and 246 W cm^{-2}, and 620 W cm^{-2}.

The third experiment, performed in the brain tissue, was designed to demonstrate that the reduced FOV EPI displacement images depict the displacement similar to in the 2D spin-warp sequence. For the same two power levels as in the previous experiment, the ultrasound transducer was defocused in four steps by addition of phase aberrations to 512, 256, 128, and 0 elements of 1024 elements of the transducer. The phase aberration values were randomly selected between $-\pi$ and π. At each of the four levels of phase aberration, three EPI-based and one 2D spin-warp–based displacement maps were obtained. In each, the displacement from a four pixel region of interest in the focal spot was measured.

The standard deviation (SD) of the noise in the displacement maps was calculated for both 2D spin-warp and EPI approaches. According to the method described in Ref. 24, the SD of noise in the phase image is inversely proportional to the signal-to-noise ratio (SNR) of the corresponding magnitude image. Therefore, the SNR values were calculated for a region of interest that covers most of the brain image and the noise SDs for the corresponding phase images were found. As the displacement image is a subtraction of two phase images, obtained with positive and negative polarities of the encoding gradient, the SD of the displacement noise is a square root of the sum of the phase noise variances.

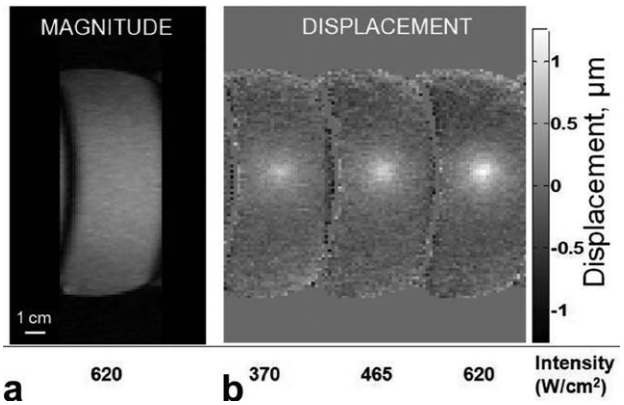

FIG. 2. Magnitude and displacement images of a phantom, obtained with EPI-based MR-ARFI using 2% duty cycle of ultrasound. **a**: A representative magnitude image obtained at 620 W cm^{-2}, indicating no sign of the focal spot. **b**: Displacement images of the phantom obtained for three values of intensity show the focal spot location and the dependence of the peak displacement on the acoustic intensity.

RESULTS

Figure 2 displays the results obtained with the limited FOV single-shot EPI MR-ARFI sequence. Overall, the images exhibit some geometric distortion caused by off-resonance effects, which are a common artifact of single-shot EPI, related to high sampling bandwidth in phase-encode direction. The focal spot is not visible on the magnitude image even for the highest intensity of 620 W cm^{-2} (Fig. 2a). However, it is very well depicted in the displacement images shown in Fig. 2b. The peak displacement increases with increasing intensity.

The results of the temperature measurements are shown in Fig. 3. The temperature maps were reconstructed for the phantom and the ex vivo brain tissue. For a 2% duty cycle, no temperature rise was detected after a single sonication either in the brain tissue or in the phantom at all of the tested intensity levels. After 3000 sonications, a temperature rise of 3.9 ± 0.7°C was measured in the phantom, as shown in Fig. 3d. The temperature increased approximately linearly for the first 500 sonications at 0.005°C sec^{-1} (or per sonication) and then was rising at much slower rate due to the heat flow (Fig. 3e).

Magnitude and displacement images obtained in brain tissue with EPI-based MR-ARFI and with 2D spin-warp–based MR-ARFI are shown in Fig. 4. Geometric distortions are observed in EPI-based images, which also have approximately three times lower magnitude SNR than the spin-warp MR-ARFI due to a longer echo time and higher bandwidth. In spite of the SNR loss, the gain in scan time duration makes the single-shot EPI approach 42 times more SNR efficient than the spin-warp method. For an EPI-based displacement map, the scan time is only 2 × TR, here 2 sec, compared with the spin-warp–based sequence where the scan time is 2 × 128 × TR, here 256 sec. The time savings we demonstrate here

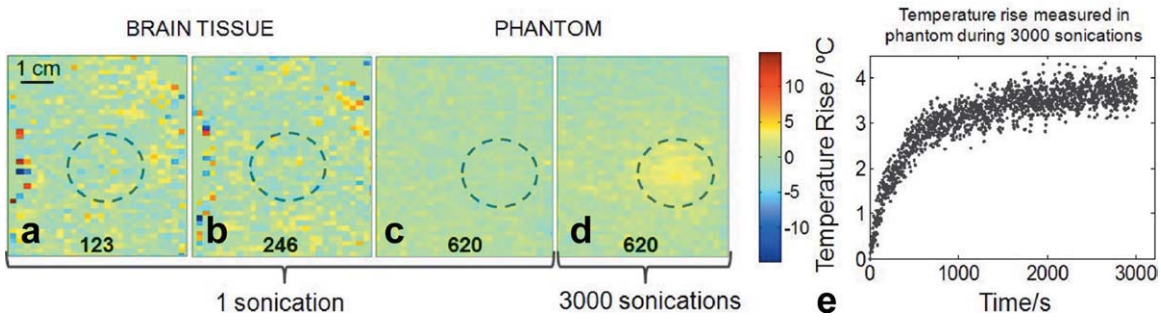

FIG. 3. Cropped temperature maps obtained in the brain tissue sample and in the phantom using the EPI-based MR-ARFI sequence, with the read-out shifted from the spin echo to introduce temperature sensitivity. Intensity levels are given in W cm^{-2} (**a–c**). No temperature rise was detected after a single sonication in the ex vivo brain tissue and in the phantom. **d**: A small temperature rise of ~4°C was measured after 3000 sonications. **e**: The temperature increased nonlinearly with sonication time.

would accelerate adaptive focusing by 128 times. Additional acceleration methods are required to bring the scan time down further from 102 min ($3 \times N \times 2 \times$ TR) to a shorter scan.

Further, the displacement maps obtained with both methods depict equally well the displacement in the focal spot, despite the much shorter scan time in the EPI-based sequence. The shear wave around the focal spot, shown with the white arrows, is detected by both imaging techniques as well.

To demonstrate the suitability of the method for adaptive focusing of the transducer, Fig. 5 shows how the phase aberrations applied to the transducer elements affect the intensity of displacement in the focal spot. The results acquired with EPI and with 2D spin-warp sequences for two different intensity levels are presented in the plot. As the phase aberrations decrease, the displacement amplitude increases linearly at the same rate for both EPI and 2D spin warp. The SD of the displacement noise averaged over 12 EPI measurements was 0.25 μm, which is three times higher than 0.08 μm measured from eight 2D spin-warp images.

DISCUSSION AND CONCLUSION

In this work, a rapid MR-ARFI method has been developed and tested in a phantom and in brain tissue. For the intensity levels used here, there was no measurable temperature rise after a single-shot EPI-based MR-ARFI acquisition. For the highest intensity of 620 W cm^{-2}, there was less than a 4°C temperature rise after 3000 continuously repeated acquisitions. Much lower intensity of 123 W cm^{-2}, sufficient to produce the displacement in the brain tissue, is not expected to cause any heating when the sonications are performed in a perfused brain in vivo. However, it would be recommended to monitor the temperature as a precaution measure during adaptive focusing procedures. The focal spot is well depicted in the displacement maps with higher SD of the noise in the EPI-based images than in 2D spin-warp images. Similarly to the results presented in the literature (25), there is some displacement detected on the periphery of the tissue. This displacement is due to the shear wave propagating away from the focal spot, and it is visible with both of the MR-ARFI techniques.

In comparison to 2D spin-warp MR-ARFI, the EPI-based MR-ARFI has lower SNR and suffers from geometric distortion. However, the distortions are a concern in localization but less so in adaptive focusing.

To improve the image quality of the EPI-based displacement images, it would be beneficial to use SENSitivity Encoding (SENSE) that has been shown to greatly reduce geometric distortion artifacts in brain imaging, by

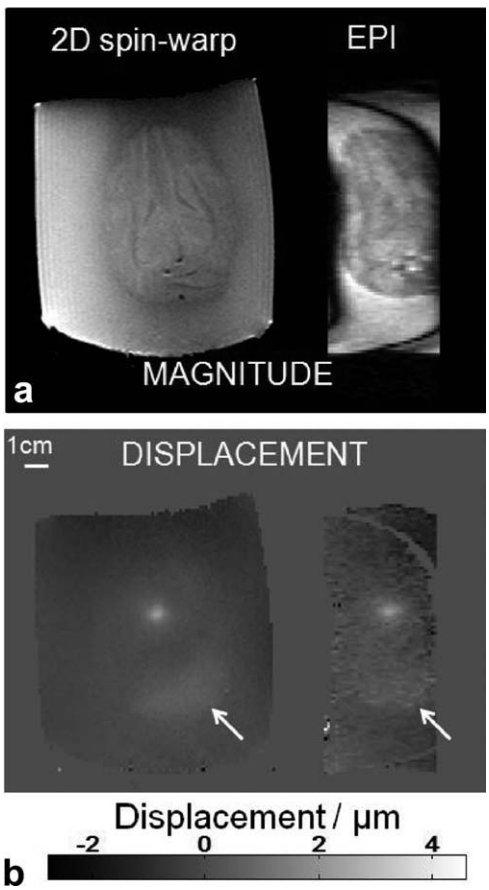

FIG. 4. Magnitude images (**a**) and displacement maps (**b**) obtained in ex vivo brain tissue with EPI-based and 2D spin-warp–based MR-ARFI. Both displacement images show the focal spot and the shear wave around the focal area, which is shown with the white arrows.

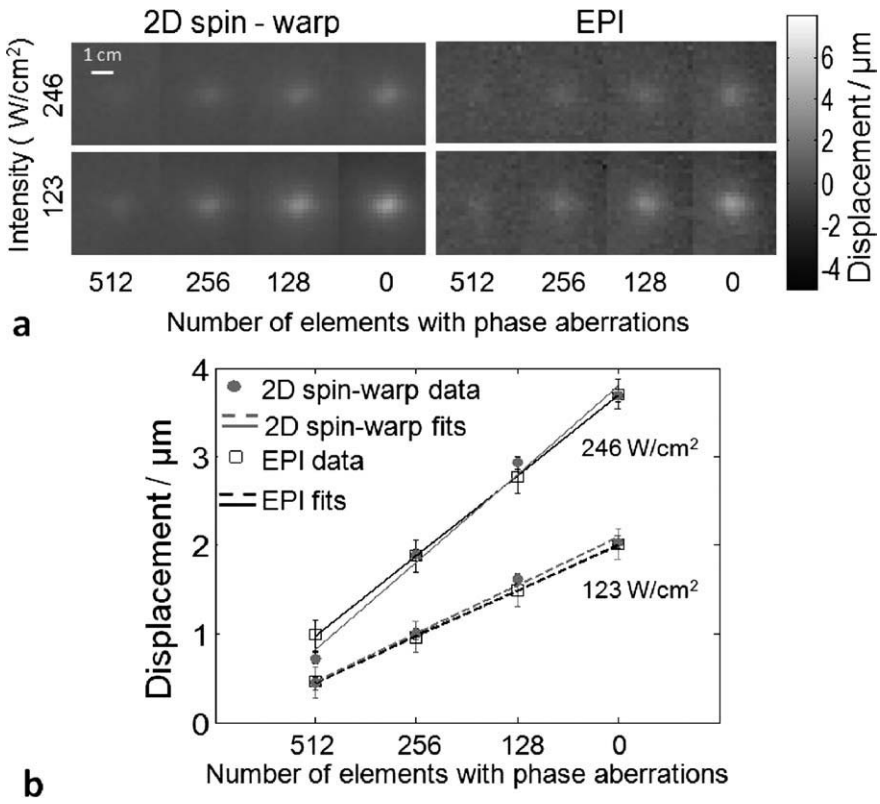

FIG. 5. **a**: Cropped displacement images obtained with varying number of defocused transducer elements for acoustic intensity of 123 and 246 W cm^{-2}. **b**: Plot of the mean displacement in the focal spot as a function of the number of the transducer elements affected by random phase aberrations. All data are displayed as mean ± SD, where displacement noise is calculated from the magnitude images. Linear fits to the data are shown with solid or dashed lines. The correlation coefficient of the fits *r* was 0.99 for both EPI and 2D spin warp.

increasing the bandwidth per pixel in the phase-encode direction, as well as to improve overall image quality by shortening the EPI train (26). In addition, implementation of SENSE would increase SNR efficiency even higher. When other imaging parameters are optimized, the total scan time duration may be traded off for a higher SNR by increasing the TR. This will also reduce the ultrasound duty cycle and slow down any potential heat accumulation. With these improvements, the single-shot EPI MR-ARFI would become a more accurate method for focal spot localization, as well as a more sensitive feedback tool for adaptive focusing in the head. Ultimately, it is envisioned that the two sequences would be used together: high resolution 2D spin warp for localization and EPI-based MR-ARFI for beam steering and adaptive focusing.

Replacing the slab excitation approach with a 2D excitation RF pulse as described in (27) would allow for multislice imaging during MR-ARFI. However, caution should be taken when doing interleaved multislice imaging, as the duty cycle will increase by the number of slices, and the total ultrasound energy delivered to the tissue over time will increase.

It has been shown (14,16) that focal spot localization based on MR-ARFI is not expected to produce tissue heating with low power levels when there is tissue perfusion. In our study, with high power levels in the phantom where there was no perfusion, the temperature rise was kept under 4°C even after 3000 sonications. This is a valuable advantage of the displacement-based visualization of the focus, when compared with the proton resonance frequency–based visualization of the low temperature rise hot spots which requires a similar temperature rise for each MR measurement. Another advantage of MR-ARFI is its lack of sensitivity to temperature changes in tissue, as long as the mechanical properties of the tissue remain constant. For example, if tissue has been heated in one or several locations after the reference phase data was collected but prior to the focal spot localization, the appearance of the test spot on the temperature maps would be obscured by the temperature rise in the surrounding or adjacent tissue, unless sufficient time passes for tissue to cool. Alternatively, a reference phase image would be necessary immediately prior to each new location of the focal spot. Rapid MR-ARFI, on the other hand, can be used as frequently as necessary to track the focal spot location, and the results will not be masked by the heat already deposited to the tissue during ablation.

In conclusion, for the first time, this study demonstrated that single-shot EPI-based MR-ARFI method can play a valuable role during MR-guided focused ultrasound procedures by reducing the imaging time and the sonication time, and at the same time provide satisfactory images of the focal spot, its location, and intensity.

ACKNOWLEDGMENTS

The authors thank InSightec Ltd. for technical support.

REFERENCES

1. Tempany CMC, Stewart EA, McDannold N, Quade BJ, Jolesz FA, Hynynen K. MR imaging-guided focused ultrasound surgery of uterine leiomyomas: a feasibility study1 10.1148/radiol.2271020395. Radiology 2003;226:897–905.
2. Hynynen K, Pomeroy O, Smith DN, Huber PE, McDannold NJ, Kettenbach J, Baum J, Singer S, Jolesz FA. MR imaging-guided focused

ultrasound surgery of fibroadenomas in the breast: a feasibility study. Radiology 2001;219:176–185.
3. Furusawa H, Namba K, Nakahara H, Tanaka C, Yasuda Y, Hirabara E, Imahariyama M, Komaki K. The evolving nonsurgical ablation of breast cancer: MR guided focused ultrasound (MRgFUS). Breast Cancer 2007;14:55–58.
4. Gianfelice D, Khiat A, Amara M, Belblidia A, Boulanger Y. MR imaging-guided focused US ablation of breast cancer: histopathologic assessment of effectiveness-initial experience1 10.1148/radiol. 2281012163. Radiology 2003;227:849–855.
5. Illing RO, Kennedy JE, Wu F, ter Haar GR, Protheroe AS, Friend PJ, Gleeson FV, Cranston DW, Phillips RR, Middleton MR. The safety and feasibility of extracorporeal high-intensity focused ultrasound (HIFU) for the treatment of liver and kidney tumours in a Western population. Br J Cancer 2005;93:890–895.
6. Hynynen K, McDannold N, Clement G, Jolesz FA, Zadicario E, Killiany R, Moore T, Rosen D. Preclinical testing of a phased array ultrasound system for MRI-guided noninvasive surgery of the brain—a primate study. Eur J Radiol 2006;59:149–156.
7. Martin E, Jeanmonod D, Morel A, Zadicario E, Werner B. High-intensity focused ultrasound for noninvasive functional neurosurgery. Ann Neurol 2009;66:858–861.
8. McDannold N, Clement G, Zadicario E, Black P, Jolesz FA, Hynynen K. Transcranial MRI-guided focused ultrasound surgery of brain tumors: initial findings in patients. In: Proceedings of the 17th Annual Meeting of ISMRM, Honolulu, 2009. p 446.
9. O'Donnell M, Flax SW. Phase aberration measurements in medical ultrasound: human studies. Ultrason Imaging 1988;10:1–11.
10. Tanter M, Thomas J-L, Fink M. Focusing and steering through absorbing and aberrating layers: application to ultrasonic propagation through the skull. J Acoust Soc Am 1998;103:2403–2410.
11. Clement GT, Hynynen K. A noninvasive method for focusing ultrasound through the human skull. Phys Med Biol 2002;47: 1219–1236.
12. King R, Rieke V, Pauly KB. Effect of the rat skull on focused US, as measured by MR thermometry. In: Proceedings of 9th International Symposium of Therapeutic Ultrasound, Aix-en-Provnce, France, 2009. pp 387–390.
13. Ishihara Y, Calderon A, Watanabe H, Okamoto K, Suzuki Y, Kuroda K, Suzuki Y. A precise and fast temperature mapping using water proton chemical shift. Magn Reson Med 1995;34:814–823.
14. McDannold N, Maier SE. Magnetic resonance acoustic radiation force imaging. Med Phys 2008;35:3748–3758.
15. Huang Y, Curiel L, Kukic A, Plewes DB, Chopra R, Hynynen K. MR acoustic radiation force imaging: in vivo comparison to ultrasound motion tracking. Med Phys 2009;36:2016–2020.
16. Larrat B, Pernot M, Aubry J-F, Dervishi E, Sinkus R, Seilhean D, Marie Y, Boch A-L, Fink M, Tanter M. MR-guided transcranial brain HIFU in small animal models. Phys Med Biol 2010;55:365–388.
17. Chen J, Watkins R, Pauly KB. Optimization of encoding gradients for MR-ARFI. Magn Reson Med 2010;63:1050–1058.
18. Kaye E, Chen J, Pauly KB. Rapid MR-ARFI method for focal spot localization during focused ultrasound treatments. In: Proceedings of pth International Symposium of Therapeutic Ultrasound, Aix-en-Provence, France, 2009. pp 247–250.
19. Larrat B, Pernot M, Montaldo G, Fink M, Tanter M. Energy-based adaptive focusing: optimal ultrasonic focusing using magnetic resonance guidance. In: Hynynen K, Souquet J, editors: AIP; 2010. pp 140–144.
20. Hertzberg Y, Volovick A, Zur Y, Medan Y, Vitek S, Navon G. Ultrasound focusing using magnetic resonance acoustic radiation force imaging: application to ultrasound transcranial therapy. Med Phys 2010;37: 2934–2942.
21. Jensen JA. Calculation of pressure fields from arbitrarily shaped, apodized, and excited ultrasound transducers. IEEE Trans Ultrason Ferroelectr Freq Control 1992;39:262–267.
22. Jensen JA. Field: a program for simulating ultrasound systems. Med Biol Eng Comput 1996;34 (S1):351–353.
23. Duck FA. Physical properties of tissue. A comprehensive reference book. London: Academic Press; 1990. pp 72–135.
24. Gudbjartsson H, Patz S. The rician distribution of noisy MRI data. Magn Reson Med 1995;34:910–914.
25. Wu T, Felmlee JP, Greenleaf JF, Riederer SJ, Ehman RL. MR imaging of shear waves generated by focused ultrasound. Magn Reson Med 2000;43:111–115.
26. Bammer R, Keeling SL, Augustin M, Pruessmann KP, Wolf R, Stollberger R, Hartung H-P, Fazekas F. Improved diffusion-weighted single-shot echo-planar imaging (EPI) in stroke using sensitivity encoding (SENSE). Magn Reson Med 2001;46:548–554.
27. Saritas EU, Cunningham CH, Lee JH, Han ET, Nishimura DG. DWI of the spinal cord with reduced FOV single-shot EPI. Magn Reson Med 2008;60:468–473.